AIMS Materials Science, 5(2): 171–189.
DOI: 10.3934/matersci.2018.2.171
Received: 12 December 2017
Accepted: 22 February 2018
Published: 06 March 2018

http://www.aimspress.com/journal/Materials

Research article

Hydrophilic surfaces via the self-assembly of nitrile-terminated alkanethiols on gold

Chul Soon Park[1], Oussama Zenasni[1], Maria D. Marquez[1], H. Justin Moore[2,*] and T. Randall Lee[1,*]

[1] Departments of Chemistry and Chemical Engineering and the Texas Center for Superconductivity, University of Houston, Houston, Texas 77204, United States
[2] Department of Chemistry, University of Texas Rio Grande Valley, One West University Blvd., Brownsville, Texas 78520, United States

* **Correspondence:** Email: justin.moore@utrgv.edu; Tel: +956-882-5737; Email: trlee@uh.edu; Tel: +713-743-2724; Fax: +281-754-4445.

Abstract: A series of CN-terminated alkanethiols were synthesized and used to generate self-assembled monolayers (SAMs) on gold. The SAMs were characterized using ellipsometry, contact angle goniometry, polarization modulation infrared reflection absorption spectroscopy (PM-IRRAS), and X-ray photoelectron spectroscopy (XPS). The SAMs were compared to those derived from a series of analogous CH_3-terminated alkanethiols. The CN-terminated SAMs exhibited lower film thicknesses than the CH_3-terminated SAMs, which was largely due to their greater tilt angle on the surface. Additionally, the CN-terminated SAMs form well-ordered films on flat gold surfaces with relative packing densities being indistinguishable from the CH_3-terminated SAMs. The CN-terminated SAMs exhibited a less hydrophobic character than the SAMs derived from CH_3-terminated adsorbates, which was attributed to the dipole moment of the terminal group as well as the lone pair of the nitrogen atom of the CN-terminal group.

Keywords: self-assembled monolayers; CN-terminated; contact angles; hydrophilic surfaces

1. Introduction

The discovery of self-assembled monolayers (SAMs) in the early 1980s by Nuzzo and Allara provided a means in which to fabricate organic surfaces with definite chemical identities and explicit interfacial properties [1]. Surfaces generated from functionalized SAMs have been applied for many chemical, physical, and biological processes such as: corrosion [2], protein or cell adhesion [3], crystal growth [4], DNA loading and releasing [5], wetting [6], friction [7], and so forth. Substantial attention has focused on using SAMs as model systems to examine specific surface properties to reveal the origin of the interactions of the aforementioned processes occurring at organic interfaces [8–10]. SAMs generally consist of a headgroup that binds to the substrate, a tailgroup representing the film interface, and a hydrocarbon spacer linking the head and tail groups [8]. The molecular structure and packing density of SAMs, in most instances, are established by the headgroup-substrate and intermolecular interactions [9,11,12], whereas the tailgroup is largely responsible in determining the vast majority of the monolayer's surface properties [9,10,11,13]. The combination of having an enormous array of compatible terminal functionalities along with the ability to manipulate the molecular architecture makes SAMs increasingly useful in scientific and practical applications [5,14–16].

Numerous studies have examined the interfacial, chemical, and structural properties of ω-terminated alkanethiolate SAMs on gold substrates [7,10–12], which include ω-terminated SAMs having systematically varied hydrocarbon backbone lengths in an effort to provide further insight into the well-known "odd-even" effect [17–19]. Some recent examples include SAMs with a phenyl [20] or trifluoromethyl [21] terminal group, all of which exhibit unique "odd-even" effects as a result of the orientation of the terminal moiety [18,19]. Taking into account the polarity of acetonitrile, the introduction of a nitrile group at the SAM interface generates a surface composed of oriented dipoles. The orientation of the dipole should depend on whether the hydrocarbon backbone contains an even or odd number of methylene units, similar to the surface dipole found in CF_3-terminated SAMs [21]. Wettability measurements conducted on the CF_3-terminated SAMs with polar liquids showed a lower advancing contact angle on SAMs having an odd number of methylene units and a higher advancing contact angle on SAMs having an even number of methylene units [21]. The "odd-even" effect observed in the wettability of CF_3-terminated SAMs was attributed to the orientation of the dipoles present at the SAM interface [21].

Nitrile-terminated SAMs have potential applications in microcontact printing (soft lithography), a technique based on printing and molding patterns using elastomeric stamps. For example, a mixed monolayer can be patterned on a gold surface by two alkanethiols terminated with different functionalities; one microprinted from a stamp, while the other post adsorbed from solution [22]. For the specific example above, patterns can be made that consist of regions with entirely different characteristics based on the interfacial and structural properties of the terminal groups, CH_3- and CN-groups. The patterned surface, can then be used to grow polymer patterns by taking advantage of the coordinating ability of Pd(II) to the CN-termini [22]. In addition to serving as microcontact printing inks, CN-terminated SAMs also serve as a great candidate for the preparation of patterned surfaces for chemical lithography as well as for nanofabrication by electron irradiation [23].

In this study, a series of nitrile-terminated alkanethiols of the form $CN(CH_2)_nSH$, where n = 14–17 (**CNCnSH**, shown in Figure 1), were synthesized and used to make SAMs. The SAMs formed from the nitrile-terminated adsorbates were characterized and compared to those derived from the analogous *n*-alkanethiols by using optical ellipsometry, contact angle goniometry, polarization modulation infrared reflection absorption spectroscopy (PM-IRRAS), and X-ray photoelectron spectroscopy (XPS).

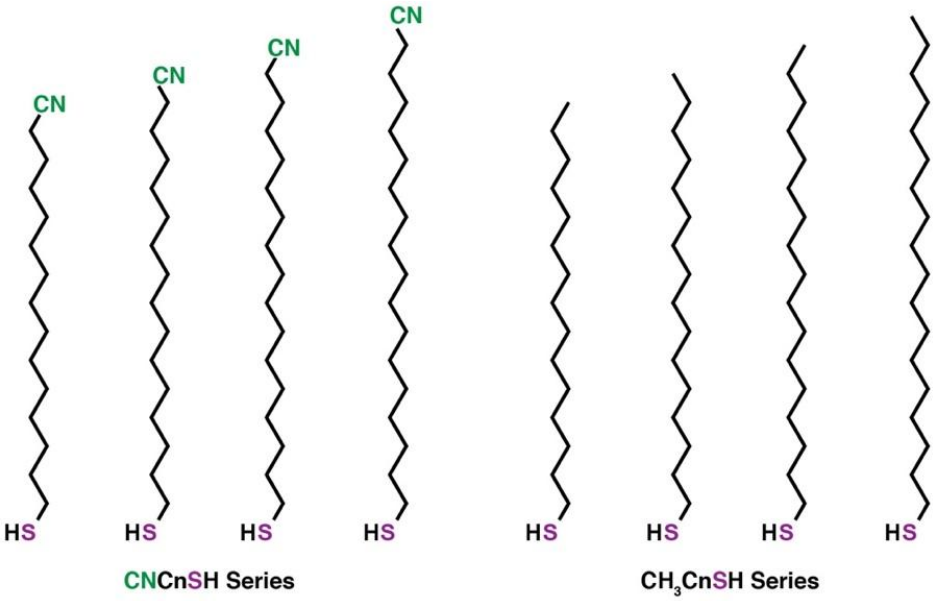

Figure 1. Adsorbates used in this study: **CNCnSH** and **CH_3CnSH**, where n = 14–17.

2. Materials and methods

2.1. Materials

Gold shot (99.99%) was purchased from Americana Precious Metals. Chromium rods (99.9%) were purchased from R. D. Mathis Company. Single-crystal silicon (100) wafers, which were polished on one side, were purchased from North East Silicon Technologies and rinsed with absolute ethanol (Aaper Alcohol and Chemical Co.) before use. The liquids used for contact angle measurements were of the highest purity available from Aldrich Chemical Co. and were used without purification. The *n*-alkanethiols used to generate SAMs were either commercially available or synthesized using established methods. Potassium iodide, acetone, dichloromethane, triethylamine, and hexanes were purchased from EM Sciences and used as received. Tetrahydrofuran (THF) (EM Sciences) was dried by passage through alumina and distilled to remove butylated hydroxytoluene (BHT). Allylmagnesium chloride (1.0 M), 11-bromo-1-undecanol, potassium thioacetate (KSAc), 2,2'-azobisisobutylnitrile (AIBN), sodium cyanide (NaCN), dimethyl sulfoxide (DMSO), triethylamine (NEt_3), *p*-toluenesulfonic acid (PTSA), lithium bromide (LiBr), borane tetrahydrofuran (1 M BH_3·THF), methanol (MeOH), ω-pentadecalactone, 16-hexadecanolide, dilithium tetraclorocuprate(II) (Li_2CuCl_4 in THF), and hydrobromic acid (HBr; 33% in acetic acid) were

purchased from Aldrich Chemical Co. and used as received. Oxacyclopentadecan-2-one was purchased from 1717CheMall. Methanesulfonyl chloride (MsCl), 3,4-dihydro-2H-pyran (DHP), thioacetic acid (AcSH), and potassium carbonate (K_2CO_3) were purchased from Acros Organics and used as received. 10-Bromo-1-decanol and 12-bromo-1-dodecanol were both purchased from TCI America and used as received. Lithium aluminum hydride (LAH) and 1,4-dithio-DL-threitol (DTT) were purchased from Alfa Aesar and used as received. 11-Bromo-1-undecene was purchased from Lancaster and used as received. Thin-layer chromatography (TLC) was carried out using Sorbent Technologies silica gelplates with UV254. The eluted TLC plates were analyzed in an iodine chamber. Column chromatography was carried out using silica gel (200–300 mesh) purchased from Natland International Corp. Nuclear Magnetic Resonance (NMR) spectra were recorded on a General Electric QE-300 spectrometer operating at 300 MHz for ^1H; the data were collected in $CDCl_3$ and referenced to δ 7.26.

2.2. Methods

2.2.1. Preparation of SAMs

Solutions of the CN- and CH_3-terminated alkanethiols were prepared in weighing bottles that were cleaned previously in piranha solution (7:3 H_2SO_4/H_2O_2) for 1 h [*Caution: Piranha solution reacts violently with organic materials and should be handled carefully*]. The weighing bottles were then rinsed with deionized water and absolute ethanol. The gold substrates were prepared by resistive evaporation of ca. 100 Å of chromium onto the polished surfaces of the silicon wafers, followed by the evaporation of ca. 1000 Å of gold; chromium promotes the adhesion of gold onto silicon. Deposition pressures were maintained at ca. 1×10^{-5} Torr. The freshly prepared gold-coated wafers were immediately transferred to Fluoroware containers and stored until used. The wafers were cut into slides (ca. 1 cm × 3 cm) with a diamond-tipped stylus. The slides were rinsed with absolute ethanol and blown dry with a stream of ultrapure nitrogen. Ellipsometric data for the bare gold were collected. The slides were then rinsed with ethanol and immersed in solutions of the respective nitrile-terminated alkanethiols (1 mM in ethanol) or *n*-alkanethiols (1 mM in ethanol). All substrates were allowed to equilibrate simultaneously for a period of at least 24 h. The resultant SAMs were rinsed with ethanol and blown dry with ultrapure nitrogen before immediate characterization.

2.2.2. Ellipsometric thicknesses measurements

The thicknesses of the monolayers were measured using a Rudolph Research Auto EL III ellipsometer equipped with a He-Ne laser (632.8 nm) at an incident angle of 70°. The optical constants of the bare gold substrates were measured immediately after gold deposition; a refractive index of 1.45 was assumed for all films. For a given sample, the data were averaged over three separate slides using three spots per slide (an average of nine measurements).

2.2.3. Contact angle measurements

Advancing and receding contact angles were measured using a ramé-hart model 100 contact angle goniometer. The contacting liquids, hexadecane ($C_{16}H_{34}$, HD) and water (H_2O, W), were dispensed and withdrawn with a Matrix Technologies micro-Electrapette 25. For a given sample, the data were averaged over three separate slides using three spots per slide and measuring angles from opposite edges of each drop (an average of eighteen measurements). The measurements were performed at 293 K with the pipet tip in contact with the drop.

2.2.4. Surface infrared spectroscopy

Polarization modulation infrared reflection absorption spectroscopy (PM-IRRAS) data were collected using a Nicolet MAGNA-IR 860 Fourier transform spectrometer equipped with a liquid-nitrogen-cooled mercury-cadmium-telluride (MCT) detector and a Hinds Instruments PEM-90 photoelastic modulator. The *p*-polarized light was incident at 80°. The spectra were collected for 1000 scans at a spectral resolution of 4 cm^{-1}.

2.2.5. X-ray photoelectron spectroscopy

X-ray photoelectron spectra were collected using a PHI 5700 X-ray photoelectron spectrometer equipped with a monochromatic Al Kα X-ray source (hν = 1486.7 eV) incident at 90° relative to the axis of a hemispherical energy analyzer. The spectrometer was operated at high resolution with a pass energy of 23.5 eV, a photoelectron takeoff angle of 45° from the surface, and an analyzer spot diameter of 1.1 mm. The base pressure in the chamber during measurements was 2×10^{-9} Torr, and the spectra were collected at room temperature. Ten scans were accumulated to obtain the C 1s and N 1s spectra, while five and thirty scans were accumulated to obtain the Au 4f and S 2p spectra, respectively. After collecting the data, the binding energies were referenced by setting the Au $4f_{7/2}$ binding energy to 84.0 eV. The peak intensities were quantified by standard curve-fitting software using Shirley background subtraction and Gaussian-Lorentzian profiles.

2.2.6. Synthesis of nitrile-terminated alkanethiols, **CNCnSH**, where n = 14–17

The ω-cyanoalkanethiols, **CNCnSH** (n = 14–17), were prepared using the strategies outlined in Schemes 1, 2, and 3. The three shorter ω-bromo-1-alkanols were synthesized by the acid-catalyzed ring opening of the corresponding lactones followed by reduction of the carboxylic acid functionality to the terminal alcohol, as shown in Scheme 1. Scheme 2 outlines the remainder of the synthesis for **CNCnSH** (n = 14–16). Since long-chain bi-functional organic compounds are difficult to find, and if available are generally very expensive, the **CNC17SH** was synthesized using a different route, presented in Scheme 3.

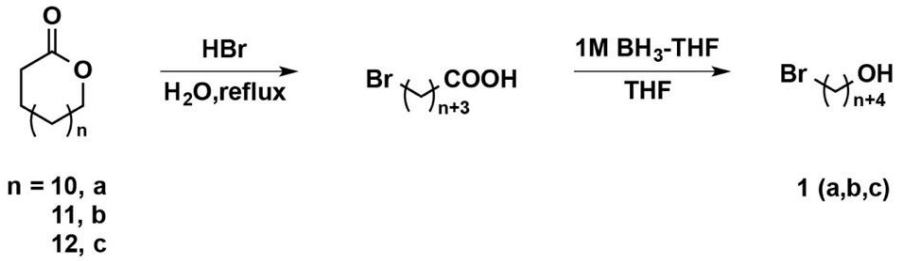

Scheme 1. Synthesis of ω-Bromoalcohols from the Corresponding Lactones.

*14-Bromo-1-tetradecanol (**1a**).* To an aliquot of oxacyclopentadecan-2-one (5.0 g, 22 mmol) was added HBr (33% in acetic acid, 74 mL) and water (50 mL). The reaction was refluxed at 130 ℃ for 24 h, cooled to room temperature, poured over cold water (250 mL) and then stirred for 1 h. The resulting brown precipitate was filtered, washed extensively with water (5 × 100 mL), and recrystallized from hexanes to afford pure 14-bromotetradecanoic acid (5.6 g, 83%) as white flakes. The resulting acid (5.6 g, 18 mmol) was dissolved in ~250 mL of THF and cooled in an ice-bath to 0 ℃. 24 mL of 1.0 M BH_3/THF solution was added to the acid slowly over 20 min and stirred vigorously for 1 h. Excess borane was then quenched with a 50/50 water/THF mixture. The aqueous layer was extracted with diethyl ether (3 × 100 mL), and the organic phase washed successively with $NaHCO_3$ (100 mL), water (100 mL), and brine (100 mL). The organic phase was dried over anhydrous $MgSO_4$, filtered, and evaporated to dryness. The crude product was recrystallized from hexanes to afford pure 14-bromo-1-tetradecanol (3.3 g, 11 mmol) in 62% yield. ^{1}H NMR (300 MHz, $CDCl_3$): δ 3.60 (t, *J* = 5.0 Hz, 2H), 3.41 (t, *J* = 6.7 Hz, 2H), 1.80–1.90 (m, 2H), 1.52–1.61 (m, 2H), 1.26 (m, 20H).

*15-Bromo-1-pentadecanol (**1b**).* Compound **1b** was synthesized using a procedure analogous to that used to synthesize compound **1a**: (3.2 g, 10 mmol, 62% yield). ^{1}H NMR (300 MHz, $CDCl_3$): δ 3.61 (t, *J* = 5.0 Hz, 2 H), 3.40 (t, *J* = 6.6 Hz, 2 H), 1.90–1.81 (m, 2 H), 1.60–1.52 (m, 2H), 1.26 (m, 22H).

*16-Bromo-1-hexadecanol (**1c**).* Compound **1c** was synthesized using a procedure analogous to that used to synthesize compound **1a**: (2.9 g, 9.0 mmol, 60% yield). ^{1}H NMR (300 MHz, $CDCl_3$): δ 3.62 (t, *J* = 5.0 Hz, 2H), 3.42 (t, *J* = 6.6 Hz, 2H), 1.82–1.90 (m, 2H), 1.51–1.61 (m, 2H), 1.26 (m, 24H).

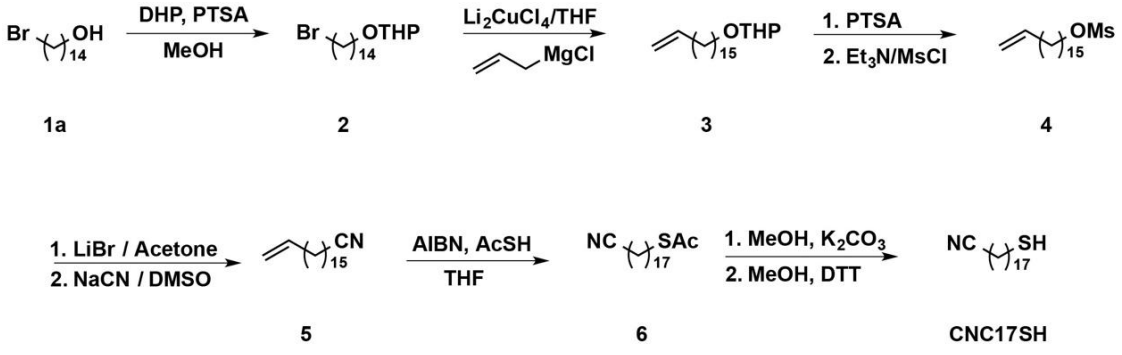

Scheme 2. Synthesis of 18-Mercaptooctandecanenitrile (**CNC17SH)**.

*2-(14-Bromo-tetradecyloxy)-tetrahydropyran (**2**).* A solution of compound **1a** (1.5 g; 5.1 mmol) and DHP (0.65 g; 7.7 mmol) in 100 mL of dry MeOH containing PTSA (0.13 g; 0.51 mmol) was stirred for 4 h at room temperature. Then, the solution was diluted with hexanes (1 × 100 mL) and washed once with half-saturated brine (1 × 100 mL) to remove the catalyst. The solution was then dried over $MgSO_4$ and the solvent removed by rotary evaporation. 2-(14-Bromo-tetradecyloxy)-tetrahydropyran (**2**, 1.83 g, 4.85 mmol) was obtained in 95% yield. ^{1}H NMR (300 MHz, $CDCl_3$); δ 4.57 (t, *J* = 4.6 Hz, 1H), 3.83–3.91 (m, 1H), 3.69–3.77 (m, 1H), 3.46–3.53 (m, 1H), 3.39–3.42 (m, 1H), 3.41 (t, *J* = 7.2 Hz, 2H), 1.70–1.90 (m, 4H), 1.49–1.61 (m, 6H), 1.22–1.41 (m, 20H).

*2-(Heptadec-16-enyloxy)-tetrahydropyran (**3**).* To a solution of compound **2** (1.8 g; 4.9 mmol) in 150 mL anhydrous THF were added 2.4 mL of a 0.1 M solution of Li_2CuCl_4 in THF (0.2 mmol). The mixture was cooled to 0 ℃ in an ice-bath under argon. Afterwards, a 2.0 M solution of allylmagnesium chloride in diethyl ether (4.9 mL; 10 mmol) was added slowly over 5 min, during which a color change from orange to dark brown occurred. The reaction mixture was warmed to room temperature and refluxed for 14 h. After the addition of 50 mL of a saturated aqueous solution of NH_4Cl and 50 mL of water, the mixture was extracted with hexanes (3 × 50 mL). The combined organic layers were washed with brine (1 × 50 mL), dried with $MgSO_4$, and evaporated to dryness by rotary evaporation. 2-(Heptadec-16-enyloxy)-tetrahydropyran (**3**, 1.4 g, 4.0 mmol) was obtained in 83% yield. ^{1}H NMR (300 MHz, $CDCl_3$); δ 5.75–5.92 (m, 1H), 4.89–5.02 (m, 2H), δ 4.58 (t, *J* = 4.5 Hz, 1H), 3.84–3.90 (m, 1H), 3.69–3.77 (m, 1H), 3.46–3.55 (m, 1H), 3.34–3.43 (m, 1H), 2.00–2.07 (m, 2H), 1.75–1.87 (m, 4H), 1.51–1.66 (m, 6H), 1.20–1.39 (m, 22H).

*Heptadec-16-enyl methanesulfonate (**4**).* A solution of compound **3** and PTSA (0.1 g; 0.4 mmol) in 100 mL of ethanol was stirred at 55 ℃ for 3 h. The solvent was then removed by rotary evaporation and the residue was chromatographed on silica gel (hexanes/ethyl acetate = 10/1). The resulting heptadec-16-en-1-ol was then dissolved in 100 mL of hexanes at room temperature. NEt_3 (1.2 g; 12 mmol) and MsCl (0.92 g; 8.1 mmol) were added while stirring. After stirring for 2 h, 75 mL of water was added. The phases were separated, the organic layer was washed with water (1 × 75 mL) and brine (1 × 75 mL), dried with $MgSO_4$, and the solvent was removed by rotary evaporation. Heptadec-16-enyl methanesulfonate (**4**, 0.94 g, 2.8 mmol) was obtained in 70% yield. ^{1}H NMR (300 MHz, $CDCl_3$); δ 5.75–5.88 (m, 1H), 4.90–5.03 (m, 2H), 4.22 (t, *J* = 6.5 Hz, 2H), 3.00 (s, 3H), 2.00–2.07 (m, 2H), 1.70–1.79 (m, 2H), 1.21–1.42 (m, 24H).

*Octadec-17-enenitrile (**5**).* Mesylate **4** (0.94 g, 2.8 mmol) and LiBr (0.73 g, 8.5 mmol) were dissolved in reagent grade acetone and refluxed overnight. Afterwards, the solvent was evaporated followed by the addition of water (100 mL) and diethyl ether (100 mL). The aqueous layer was then extracted with diethyl ether (3 × 100 mL), the combined organic layers were washed with brine (100 mL), dried over $MgSO_4$, filtered, and the solvent evaporated to dryness to afford 17-bromoheptadec-1-ene (0.86 g, 2.7 mmol) in 96% yield which was used in the next step without further purification.

To an aliquot of the bromoalkene (0.86 g, 2.7 mmol) dissolved in DMSO (100 mL) was added NaCN (0.27 g, 5.4 mmol). The mixture was heated at 80 ℃ for 12 h. Dichloromethane (100 mL) was added to the mixture and the organic layer was washed with water (100 mL) and brine (100 mL). The organic layer was then dried over $MgSO_4$, filtered, and evaporated to dryness. Octadec-17-enenitrile (**5**, 0.66 g, 2.5 mmol) was obtained in 92% yield. ^{1}H NMR (300 MHz, $CDCl_3$): δ 5.75–5.88

(m, 1H), 4.90–5.03 (m, 2H), 2.33 (t, *J* = 7.2 Hz, 2H), 2.00–2.07 (m, 2H), 1.51–1.70 (m, 4H), 1.17–1.46 (m, 22H).

*S-17-Cyanoheptadecyl ethanethioate (**6**).* Under argon, an aliquot of compound **5** (0.66 g, 2.5 mmol), AcSH (0.76 g; 10 mmol), and AIBN (0.016 g; 0.01 mmol) in THF were combined in a test tube. The reaction mixture was irradiated for 2 h with a 450 W mercury high pressure lamp at a distance of 2 in. An additional equivalent of AIBN was added to the mixture and irradiated for an additional 3 h. Afterward, the resulting solution was poured into 100 mL of hexanes. Water (50 mL) was added; solid $NaHCO_3$ was then added in portions until the evolution of CO_2 ceased. The mixture was then extracted with hexane (2 × 100 mL). The organic layers were washed with brine (100 mL), dried over $MgSO_4$, filtered, and evaporated to dryness by rotary evaporation. The crude product was chromatographed on silica gel using hexanes as the eluent. *S*-17-Cyanoheptadecyl ethanethioate (**6**, 0.52 g, 1.5 mmol) was obtained in 61% yield. ^{1}H NMR (300 MHz, $CDCl_3$); δ 2.88 (t, *J* = 7.7 Hz, 2H), 2.33 (t, *J* = 7.1 Hz, 2H), 2.32 (s, 3H), 1.50–1.70 (m, 4H), 1.21–1.46 (m, 26H).

*18-Mercaptooctadecanenitrile (**CNC17SH**).* A 500-mL round-bottom flask was charged with compound **6** (0.52 g, 1.5 mmol), sealed, and then purged with argon. MeOH (150 mL; previously degassed) and K_2CO_3 (0.62 g, 7.53 mmol) were placed in a separate 100-mL round-bottom flask and added via cannula to the *S*-17-cyanoheptadecyl ethanethioate solution; the mixture was stirred vigorously at 50 ℃ for 2 h to give a mixture of **CNC17SH** and the corresponding disulfide. An aliquot of DTT (1.16 g, 7.5 mmol) dissolved in methanol (100 mL; degassed) was added via cannula to the crude mixture and stirred at room temperature for 2 h. Following, an aliquot of ~50 mL of a 1.0 M solution of H_2SO_4 in MeOH (degassed) was added to the reaction mixture slowly. The mixture was then extracted with dichloromethane (3 × 100 mL). The combined organic layers were washed with water (100 mL), 0.1 M HCl (100 mL), brine (100 mL), dried over $MgSO_4$, filtered, and the solvent evaporated to dryness. The crude product was purified by column chromatography using hexanes as the eluent to afford pure 18-mercaptopentadecanenitrile (**CNC17SH**, 0.32 g, 1.1 mmol) in 72% yield. ^{1}H NMR (300 MHz, $CDCl_3$); δ 2.55–2.48 (q, *J* = 7.4 Hz, 2H), 2.33 (t, *J* = 7.1 Hz, 2H), 1.70–1.55 (m, 4H), 1.46–1.25 (m, 26H). ^{13}C NMR (75 MHz, $CDCl_3$): δ 119.87, 34.01, 29.53 (multiple peaks), 29.44, 29.26, 29.04, 28.72, 28.63, 28.35, 25.33, 24.64, 17.11.

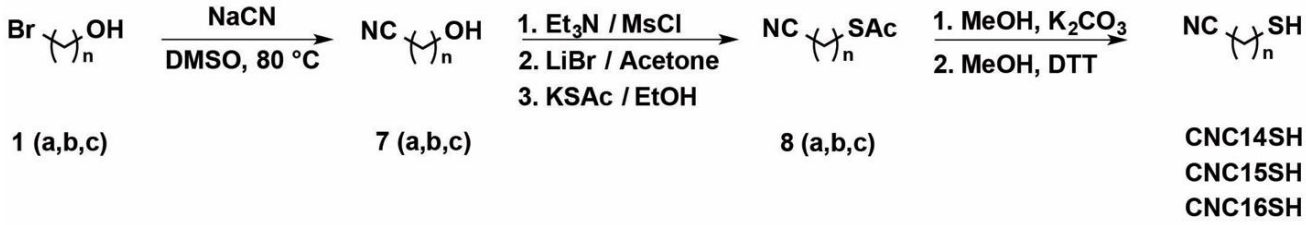

Scheme 3. Synthesis of Nitrile-Terminated Alkanethiols, **CNCnSH** (where n = 14, 15, and 16).

*14-Hydroxytetradecanenitrile (**7a**).* To an aliquot of compound **1a** (0.98 g, 3.4 mmol) dissolved in DMSO (100 mL) was added NaCN (0.33 g, 6.7 mmol). The mixture was heated at 80 ℃ for 12 h. Dichloromethane (100 mL) was added and the organic layer was washed with water (100 mL) and

brine (100 mL). The organic layer was then dried over $MgSO_4$, filtered, and evaporated to dryness. 14-Hydroxytetradecanenitrile (0.77 g, 3.2 mmol) was obtained in 96% yield. ^{1}H NMR (300 MHz, $CDCl_3$): δ 3.64 (t, *J* = 6.2 Hz, 2H), 2.61 (s, 1H), 2.33 (t, *J* = 7.3 Hz, 2H), 1.51–1.70 (m, 4H), 1.17–1.46 (m, 20H).

*15-Hydroxypentadecanenitrile (**7b**).* Compound **7b** was synthesized using a procedure analogous to that used to synthesize compound **7a**: (0.79 g, 3.1 mmol, 92% yield). ^{1}H NMR (300 MHz, $CDCl_3$): δ 3.62 (t, *J* = 6.7 Hz, 2H), 2.61 (s, 1H), 2.33 (t, *J* = 7.0 Hz, 2H), 1.51–1.70 (m, 4H), 1.16–1.42 (m, 22H).

*16-Hydroxyhexadecanenitrile (**7c**).* Compound **7c** was synthesized using a procedure analogous to that used to synthesize compound **7a**: (0.73 g, 2.7 mmol, 91% yield). ^{1}H NMR (300 MHz, $CDCl_3$): δ 3.64 (t, *J* = 6.7 Hz, 2H), 2.62 (s, 1H), 2.33 (t, *J* = 7.4 Hz, 2H), 1.51–1.70 (m, 4H), 1.18–1.43 (m, 24H).

*S-14-Cyanotetradecyl ethanethioate (**8a**).* To an aliquot of compound **7a** (0.77g, 3.2 mmol) diluted in 50 mL of hexanes was added slowly an aliquot of NEt_3 (0.98 g, 9.6 mmol). The reaction mixture was left stirring for 30 min at room temperature; the solution was then cooled in an ice-bath, and an aliquot of MsCl (0.74 g, 6.4 mmol) was added dropwise. The reaction was left stirring for 4 h at room temperature under argon. Excess MsCl was destroyed using water, and the precipitate was dissolved with water (100 mL). The aqueous layer was extracted with diethyl ether (3 × 100 mL) and the combined organic layers were washed with dilute HCl (100 mL), $NaHCO_3$ (100 mL), and brine (300 mL). The organic layer was then dried over $MgSO_4$, filtered, and evaporated to dryness.

The crude mesylate and LiBr (0.84 g, 9.6 mmol) were dissolved in acetone and refluxed overnight. The solvent was evaporated; water (100 mL) and diethyl ether (100 mL) were added to dissolve the salts and the product, respectively. The aqueous layer was extracted with diethyl ether (3 × 100 mL). The combined organic layers were washed with brine (100 mL), dried over $MgSO_4$, and evaporated to dryness. The crude bromide was flash chromatographed over silica gel using hexanes as the eluent. This product was then dissolved in ethanol (100 mL; degassed by bubbling with argon) and an aliquot of potassium thioacetate (0.74 g, 6.4 mmol) dissolved in 100 mL of ethanol (degassed) was added. The reaction was refluxed overnight under argon. The solvent was evaporated and the crude was redissolved in diethyl ether (100 mL). Water (100 mL) was added to dissolve the salts and the aqueous phase was extracted with diethyl ether (3 × 100 mL). The combined organic layers were washed with water (100 mL), brine (100 mL), dried over $MgSO_4$, filtered, and evaporated to dryness to afford *S*-14-cyanotetradecyl ethanethioate (**8a**, 0.75 g, 2.5 mmol) in 78% yield. ^{1}H NMR (300 MHz, $CDCl_3$): δ 2.86 (t, *J* = 7.7 Hz, 2H), 2.33 (t, *J* = 7.0 Hz, 2H), 2.32 (s, 3H), 1.50–1.70 (m, 4H), 1.18–1.46 (m, 20H).

*S-15-Cyanopentadecyl ethanethioate (**8b**).* Compound **8b** was synthesized using a procedure analogous to that used to synthesize compound **8a**: (0.80 g, 2.5 mmol, 83% yield). ^{1}H NMR (300 MHz, $CDCl_3$): δ 2.86 (t, *J* = 7.4 Hz, 2H), 2.33 (t, *J* = 6.8 Hz, 2H), 2.32 (s, 3H), 1.70–1.50 (m, 4H), 1.46–1.18 (m, 22H).

*S-16-Cyanohexadecyl ethanethioate (**8c**).* Compound **8c** was synthesized using a procedure analogous to that used to synthesize compound **8a**: (0.61 g, 1.9 mmol, 69% yield). ^{1}H NMR (300 MHz, $CDCl_3$): δ 2.86 (t, *J* = 7.6 Hz, 2H), 2.33 (t, *J* = 7.1 Hz, 2H), 2.32 (s, 3H), 1.70–1.50 (m, 4H), 1.48–1.18 (m, 24H).

*15-Mercaptopentadecanenitrile (**CNC14SH**).* Compound **CNC14SH** was synthesized using a procedure analogous to that used to synthesize compound **CNC17SH**: (0.57 g, 2.2 mmol, 89% yield). ^{1}H NMR (300 MHz, $CDCl_3$): δ 2.48–2.55 (q, *J* = 7.4 Hz, 2H), 2.33 (t, *J* = 7.1 Hz, 2H), 1.55–1.70 (m, 4H), 1.25–1.46 (m, 20H). ^{13}C NMR (75 MHz, $CDCl_3$): δ 119.87, 34.01, 29.53 (multiple peaks), 29.44, 29.26, 29.04, 28.72, 28.63, 28.35, 25.33, 24.64, 17.11.

*16-Mercaptohexadecanenitrile (**CNC15SH**).* Compound **CNC15SH** was synthesized using a procedure analogous to that used to synthesize compound **CNC17SH**: (0.49 g, 1.8 mmol, 71% yield). ^{1}H NMR (300 MHz, $CDCl_3$): δ 2.48–2.55 (q, *J* = 7.4 Hz, 2H), 2.33 (t, *J* = 7.1 Hz, 2H), 1.55–1.70 (m, 4H), 1.25–1.46 (m, 22H). ^{13}C NMR (75 MHz, $CDCl_3$): δ 119.87, 34.01, 29.58 (multiple peaks), 29.55, 29.48, 29.26, 29.04, 28.74, 28.63, 28.35, 25.34, 24.65, 17.11.

*17-Mercaptoheptadecanenitrile (**CNC16SH**).* Compound **CNC16SH** was synthesized using a procedure analogous to that used to synthesize compound **CNC17SH**: (0.37 g, 1.3 mmol, 69% yield). ^{1}H NMR (300 MHz, $CDCl_3$): δ 2.55–2.48 (q, *J* = 7.4 Hz, 2H), 2.33 (t, *J* = 7.1 Hz, 2H), 1.70–1.55 (m, 4H), 1.46–1.25 (m, 24H). ^{13}C NMR (75 MHz, $CDCl_3$): δ 119.87, 34.01, 29.53 (multiple peaks), 29.44, 29.26, 29.04, 28.72, 28.63, 28.35, 25.33, 24.64, 17.11.

3. Results and discussion

3.1. Ellipsometric thicknesses

Figure 2 shows the ellipsometric thicknesses of the SAMs on evaporated gold formed from the *ω*-nitrilealkanethiols and the corresponding *n*-alkanethiols having analogous chain lengths. As the number of methylene units increased from 14 to 17 for the CN-terminated adsorbates, the thicknesses systematically increased. By calculating the slope of each curve, the length per methylene unit of the two SAMs can be estimated. The plot of the CH_3-terminated SAMs gives a slope of 1.58 Å per methylene unit, whereas the plot for the CN-terminated SAMs gives a slope of 1.36 Å per methylene unit. The calculated slope and the observed thicknesses of the CH_3-terminated SAMs are consistent with the literature [24]. However, a direct comparison of the CH_3- and the CN-terminated SAMs reveals that the thicknesses of the SAMs derived from the CN-terminated alkanethiols are approximately 1.0–1.5 Å lower than the SAMs derived from the *n*-alkanethiols. Furthermore, the thickness of the SAM derived from **CNC17SH** appears anomalously low. While SAMs derived from *n*-alkanethiols are well-defined and known to have an alkyl chain tilt of ~30 ° from the surface normal [13,25], the obtained thicknesses and the smaller calculated slope of the CN-terminated SAMs indicates a larger tilt angle for the chains [26]. Additionally, for the CN-terminated SAMs, the terminal CN-groups might influence the structure of the monolayer. For this system, the electrostatic interactions between the CN-termini at the interface of the film are likely causing the carbon backbone to tilt additionally from the surface normal [26,27].

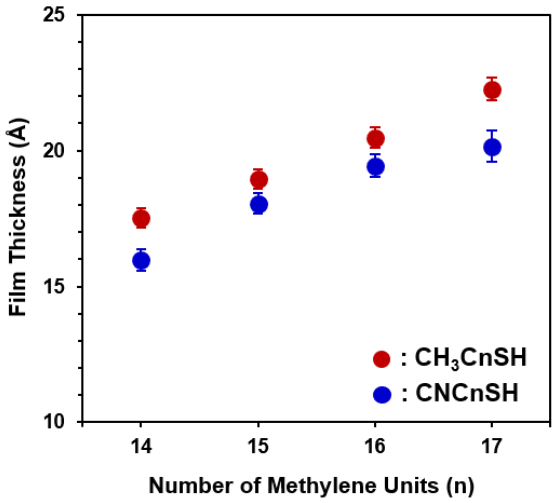

Figure 2. Ellipsometric thicknesses of SAMs formed from **CH_3CnSH** (red) and **CNCnSH** (blue) on flat gold surfaces.

3.2. Wettability of the films

To examine the wettability of the SAMs formed from the *ω*-nitrilealkanethiols and *n*-alkanethiols, we chose a variety of contacting liquids: water, N,N-dimethylformamide, acetonitrile, nitrobenzene, perfluorodecalin, methylformamide, decalin, and squalene in an attempt to observe "odd-even" effects that might exist due to the orientational differences of the terminal functional groups [19,21]. Unfortunately, only water gave measurable advancing contact angles for the CN-terminated SAMs (see Figure 3); average values obtained for these SAMs were 75 ± 2 °.

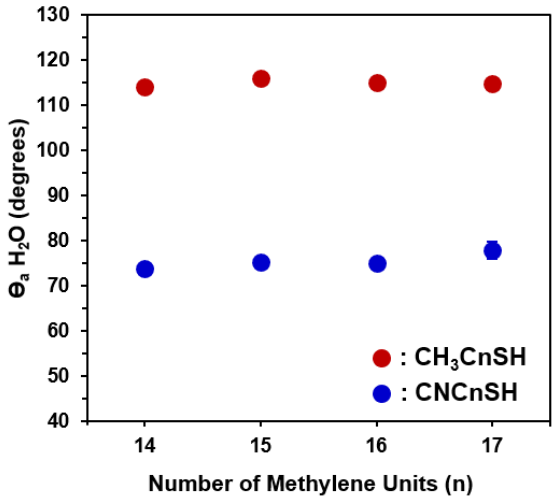

Figure 3. Advancing contact angles of water ($\theta_a^{H_2O}$) as a function of chain length for SAMs formed from **CH_3CnSH** (red) and **CNCnSH** (blue) on flat gold surfaces. The symbols are larger than the error bars for the data points in which no error bars are visible.

Interestingly, no "odd-even" effects were observed for the CN-terminated SAMs or the CH_3-terminated SAMs (see Figure 3); for CH_3-terminated SAMs, the absence of odd-even wettability effects when using polar protic probe liquids such as water and glycerol has been attributed to the fact that these liquids are highly self-associated by hydrogen bonding [18]. Another aspect to note in Figure 3, is the decreased hydrophobic character of the CN-terminated SAMs when compared to the corresponding CH_3-terminated SAMs, which exhibit advancing contact angles of 115 ± 2 °. A hydrophilic surface is defined as having a contact angle of water that is less than 90 °[28]. Given that the advancing contact angle of water on our CN-terminated SAMs is ~75 ° (see Figure 3), it is appropriate to describe the surfaces of these SAMs as "hydrophilic". Furthermore, comparison of our CN-terminated SAMs with charged surfaces (i.e., SAMs terminated with SO_3^-, $(CH_3)_3N^+$, and NH_3^+ groups) reveals water contact angles of ~48 °, ~52 °, and ~76 °, respectively [29–31]. Based upon these comparisons, our CN-terminated SAMs are most comparable in wettability to NH_3^+-terminated SAMs. The lower water contact angles on the CN-terminated SAMs can be attributed to the presence of the dipole associated with the nitrile group, specifically the free lone pair of the nitrogen atom [26].

3.3. Analysis of SAMs by PM-IRRAS

Infrared reflectance spectroscopy is a useful tool that gives insight into the conformation of the alkyl chains within a SAM [32–34]. The degree of order for a *n*-alkanethiol SAM can be evaluated by the band position of the antisymmetric C–H stretching vibration of the methylene ($\nu_a^{CH_2}$) [33,34]. For example, the $\nu_a^{CH_2}$ of a highly ordered octadecanethiol SAM appears at ~2919 cm^{-1}, while a loosely packed SAM exhibits a $\nu_a^{CH_2}$ at ~2924 cm^{-1} [33,34]. The PM-IRRAS spectra of the C–H region obtained from the CN- and CH_3-terminated SAMs are presented in Figure 4. All of the SAMs formed from the CH_3- and CN-terminated thiols have their $\nu_a^{CH_2}$ at ~2918 cm^{-1}, which is consistent with well-ordered, predominantly all-trans extended alkyl chains [32–34]. Generally, the $\nu_a^{CH_2}$ band position remains constant at ~2918 cm^{-1} for SAMs generated from *n*-alkanethiols having 11–21 carbon atoms in their methylene backbones [33]. According to our results, there is no apparent shift in the $\nu_a^{CH_2}$ band position from 2918 cm^{-1} for the CH_3- or CN-terminated SAMs; instead there is an observed increase in the intensity of the $\nu_a^{CH_2}$ band with an increase in the number of methylene units (see Figure 4). These results are consistent with similar observations in the literature [33].

As expected, there were no detectable CH_3 vibrational modes in the spectra of the CN-terminated SAMs due to the absence of CH_3 groups in the CN-terminated adsorbates. In order to examine the vibration modes of the C–N bond, spectra were also obtained in the lower frequency region (2100–2400 cm^{-1}). Unfortunately, the C–N stretching vibration, which should arise at approximately 2250 cm^{-1}, was not detected in the IR spectra of any of the CN-terminated SAMs. The lack of C–N stretching vibrations can be explained by the structural features of the SAM and the surface selection rules that govern the PM-IRRAS technique. In a study conducted by Frey et al., near-edge X-ray absorption fine structure spectroscopy (NEXAFS) was conducted on SAMs derived from **CNC16SH** on Au and estimated the average tilt angle of the alkyl chains at approximately 42 ° from the surface normal [26]; a larger value when compared to *n*-alkanethiol SAMs of approximately 30 °(*vide supra*). In addition, the same study found the tilt angles of the CN-moieties to be ~65 ± 5 °, with respect to the surface normal, suggesting that the terminal CN groups lie predominantly along

the surface plane [26]. Hence, the dipole moment arising from the C–N stretch in these SAMs will also be along the surface plane and will not be detected by the IR technique, since only vibrations with dipole moments that are perpendicular to the substrate will be observed in the spectra. For the SAMs derived from **CNC15SH** and **CNC17SH**, the CN groups should adopt an orientation more perpendicular to the surface, and therefore, the resulting dipole moment should be detected. However, there were no detectable peaks attributed to the C–N stretch. The absence of C–N stretches in the spectra of the CN-terminated SAMs is indicative of a surface structure that is dominated by the strong electrostatic interactions between the terminal CN groups, which possibly forces the CN moieties to adopt a planar surface orientation regardless of the methylene spacer length [26].

Although it might seem contradictory that the CN-terminated SAMs can be both tilted more than CH_3-terminated SAMs but still have conformationally ordered alkyl tailgroups, it is important to remember that SAMs on gold tilt to maximize their chain-chain van der Waals interactions [35]; consequently, it is plausible to have densely packed (and conformationally ordered) methylene backbones in films that are highly tilted (vide infra).

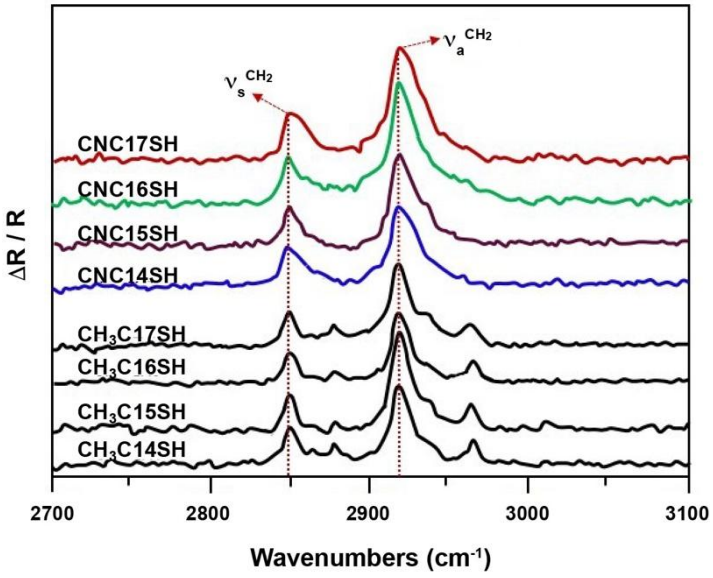

Figure 4. PM-IRRAS spectra of SAMs formed from **CH_3CnSH** and **CNCnSH** on flat gold surfaces.

3.4. Analysis of SAMs by XPS

X-ray photoelectron spectroscopy can provide crucial information such as the chemical compositions of the monolayers as well as the nature of the sulfur-gold bond [17,36]. The Au 4f, C 1s, N 1s, and S 2p spectra are presented in Figure 5. For all of the SAMs, the Au $4f_{7/2}$ peak was set to 84.0 eV, as shown in Figure 5A. In Figure 5B, the large peak centered at ~285 eV in the C 1s photoelectron region is attributed to the carbon atoms constituting the hydrocarbon backbone; a small shoulder is observed at ~286.9 eV, which is assigned to the nitrile carbon (CN) [26]. The carbon atom of the nitrile group is directly attached to the more electronegative nitrogen atom causing a shift

to a higher binding energy [26]. Additional evidence supporting the presence of the nitrile group within the SAMs can be seen in the XPS spectra of the N 1s region, shown in Figure 5C; a peak representative of the nitrogen atom of a nitrile group is centered at ~400.1 eV for all of the CN-terminated SAMs [26,37]. The results obtained from the C 1s and N 1s spectra allows for confirmation of the presence of the nitrile moiety within the films analyzed. Furthermore, the binding energy of an electron is dependent on the electron density, oxidation state, and the atoms directly attached to the atom of interest. In the case of SAMs on gold, an analysis of the S 2p peak binding energy can determine the existence of incomplete binding of an adsorbate and/or the presence of any oxidized sulfur species. For a bound thiolate, the S 2p peak appears as a doublet at ~163.2 eV (S $2p_{1/2}$) and ~162 eV (S $2p_{3/2}$), respectively [36]. An unbound or oxidized sulfur species appears at ~163–164 eV and above 166 eV, respectively [36,38,39]. The overall quality of a SAM can be determined by carefully examining the indicated regions in the S 2p spectrum. As presented in Figure 5D, all of SAMs formed from the CN-terminated adsorbates are mostly bound to the gold surfaces, and there are no highly oxidized sulfur species above 166 eV [36,39,40].

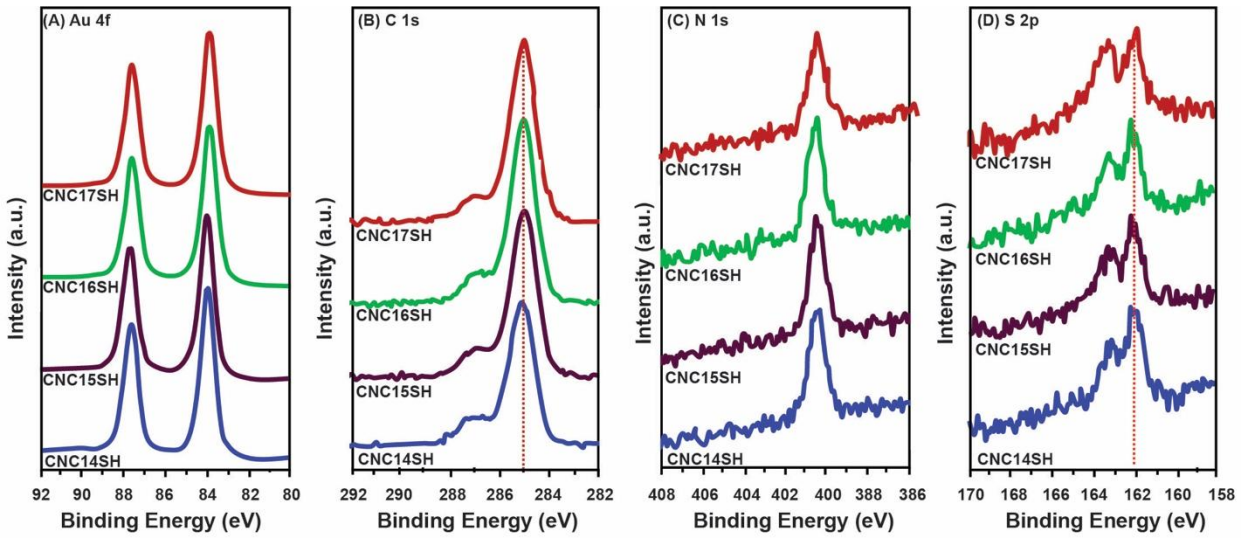

Figure 5. X-ray photoelectron spectra of the (A) Au 4f, (B) C 1s, (C) N 1s, and (D) S 2p regions of the CN-terminated SAMs with different alkyl chain lengths.

XPS can also be useful in evaluating the relative atomic composition present in a monolayer film [41,42]. Since the experimentally measured intensities of Au are dependent on the thickness of the carbon-based adsorbate, a comparison of the relative intensities of Au and C can provide information regarding the packing densities of the SAMs on gold [3,42]. An estimate of relative adsorbate surface coverage of a SAM by XPS requires a calibration of the photoelectron intensities of *n*-alkanethiol films having a known overlayer thickness. This type of quantitative analysis is dependent on the attenuation of the integrated Au 4f peak intensities by the overlaying molecules. Since the measured intensities of Au and C depend on the amount of overlying material, adsorbate alkyl chain densities can be estimated by comparing the data collected for the CN-terminated SAMs with the standard intensities observed for *n*-alkanethiol films having thicknesses and packing

densities that are precisely known [43,44]. An analysis of this sort requires the knowledge of the absolute value of the photoelectron attenuation length (λ) [41]. This can be acquired by constructing a calibration curve from the natural logarithm of the observed Au 4f intensities versus the number of carbon atoms per adsorbate from a series of SAMs generated from *n*-alkanethiols of increasing chain length (*n*-C10, *n*-C12, *n*-C14, *n*-C16, and *n*-C18). The attenuated Au 4f signal is described by Eq 1:

$$\ln Au_n = -nd/(\lambda \sin\theta) + \text{constant} \quad (1)$$

where Au_n is the intensity of the Au 4f signal attenuated by an *n* carbon monolayer, *d* is the thickness of the SAM per methylene unit, λ is the attenuation length, and θ is the takeoff angle. We assumed that the attenuation by sulfur was equivalent to 1.5 carbon atoms per adsorbate. A least-squares analysis of the Au 4f signals attenuated by the overlying *n*-alkanethiols yielded an attenuation length of 41 Å, in close agreement with the value obtained by Bain et al. [41]. We then derived an "effective" number of carbon atoms per adsorbate from the calibration curve and the measured attenuated gold signal from the CN-terminated SAMs. Then, we compared the "effective" number of carbon atoms per adsorbate with the actual stoichiometric number of carbon atoms per adsorbate in the CN-terminated SAMs. Alkyl chain densities of the CN-terminated SAMs relative to the normalized, densely packed *n*-alkanethiol SAMs are shown in Table 1; the relative chain densities of the CN-terminated series, determined from the Au 4f region, is shown along with the integrated peak areas and binding energies in Table 1.

Table 1. XPS Binding Energies, Integrated Photoelectron Intensities (counts), and Relative Packing Densities of SAMs formed from **CNC14SH**, **CNC15SH**, **CNC16SH**, and **CNC17SH**.

Element		**CNC14SH**	**CNC15SH**	**CNC16SH**	**CNC17SH**
Au 4f	count	200340	192620	188600	189320
	BE (eV)	84.0	84.0	84.0	84.0
C 1s	count	19160	22280	23500	22500
	BE (eV)	285.1, 286.8	285.0, 286.8	285.0, 286.8	285.0, 286.8
N 1s	count	2200	2550	2720	2110
	BE (eV)	400.1	400.2	400.1	400.3
S 2p	count	1750	2070	1900	2760
	BE (eV)	161.0	161.0	161.0	161.0
chain density from Au 4f (%)		97	98	97	90
S 2p/Au 4f		0.0087	0.011	0.010	0.0146

Quantitative analysis of the Au 4f peak intensities of SAMs formed from **CNC14SH**, **CNC15SH**, **CNC16SH** and **CNC17SH** revealed that these films possessed 97, 98, 97, and 90%, respectively, of alkyl chain density relative to the corresponding *n*-alkanethiol SAMs normalized to 100% packing. SAMs generated from **CNC14SH**, **CNC15SH**, and **CNC16SH** suggest that the packing densities are nearly identical to the *n*-alkanethiol SAMs and are consistent throughout the

series of chain lengths with the exception of the **CNC17SH**. The considerably lower packing densities observed in the **CNC17SH** SAMs are peculiar to say the least. The integrated photoelectron counts of Au 4f, C 1s, N 1s, and S 2p for **CNC17SH** show an abnormal relationship with the CN-terminated series. We would expect the **CNC17SH** Au 4f photoelectron counts (189320) be attenuated more than the **CNC16SH** SAMs (188600), which have a thinner carbon overlayer above the gold substrate. Likewise, we would expect the **CNC17SH** C 1s integrated photoelectron counts (22500) to be higher than the **CNC16SH** SAMs (23500) given that the **CNC17SH** SAM has one more carbon atom along the hydrocarbon chain. Additionally, the considerably higher S 2p integrated photoelectron counts for **CNC17SH** (2760) are greatly augmented in comparison to **CNC14SH** (1750), **CNC15SH** (2070), and **CNC16SH** (1900) SAMs. Moreover, the density of surface thiolates, estimated from the S 2p/Au 4f ratios, suggests greater ratios of sulfur containing moieties are present within the **CNC17SH** SAM assembly.

Taken as a whole, the XPS data help to rationalize the lower observed film thickness of **CNC17SH** SAMs, determined from the ellipsometry data, and the slightly higher advancing contact angles of water ($\theta_a^{H_2O}$) on the SAMs derived from **CNC17SH** (~3 °). We propose that the minor anomalies observed for the **CNC17SH** SAMs are due to the presence of trace amounts of dithiothreitol (DTT), which was used in the reduction of the thiol/disulfide mixture to give **CNC17SH** as the final product (see Scheme 2). The presence of trace amounts of DTT can plausibly lead to (1) a decrease in the ellipsometric thickness given the short chain length of DTT, (2) an increase in the contact angle of water by exposing underlying hydrocarbon groups, which are inherently more hydrophobic than CN moieties, and (3) an increase in the S 2p count (and the S/N ratio) as measured by XPS.

4. Conclusions

A series of CN-terminated alkanethiols having the formula of **$CN(CH_2)_nSH$** (where n = 14–17) were synthesized and used to form SAMs on flat gold surfaces to compare with SAMs derived from the analogous *n*-alkanethiols **$CH_3(CH_2)_nSH$** (where n = 14–17). The SAMs were characterized using ellipsometry, contact angle goniometry, surface IR spectroscopy (PM-IRRAS), and XPS. The analyses by PM-IRRAS and XPS found that the conformational order and the packing density, respectively, of the CN-terminated SAMs were largely indistinguishable from the SAMs derived from *n*-alkanethiols. Surface IR spectra indicate that CN-terminated alkanethiols generate conformationally ordered films; however, the C–N stretch was not observed. Strong electrostatic interactions at the surface plausibly perturb the CN group from adopting a terminal conformation that is parallel to the substrate, eliminating the ability of the PM-IRRAS technique to detect the C–N vibration. However, CN-terminated films generate hydrophilic surfaces that satisfy the four criteria used for the generation of inert surfaces that can resist the adsorption and adhesion of biological species: (1) high polarity, (2) lack of hydrogen bond donors, (3) presence of hydrogen bond acceptors, and (4) they are electrically neutral.

Acknowledgments

The National Science Foundation (CHE-1411265 and CHE-1710561), the Robert A. Welch Foundation (E-1320), and the Texas Center for Superconductivity at the University of Houston provided generous support for this research. Collaborative research efforts at the University of Texas Rio Grande Valley were also generously supported by the Robert A. Welch Foundation (BX-0048).

Conflict of interest

The authors declare that there is no conflict of interest regarding the publication of this manuscript.

References

1. Nuzzo RG, Allara DL (1983) Adsorption of bifunctional organic disulfides on gold surfaces. *J Am Chem Soc* 105: 4481–4483.
2. Whelan CM, Kinsella M, Carbonell L, et al. (2003) Corrosion inhibition by self-assembled monolayers for enhanced wire bonding on Cu surfaces. *Microelectron Eng* 70: 551–557.
3. Ostuni E, Chapman RG, Liang MN, et al. (2001) Self-assembled monolayers that resist the adsorption of proteins and the adhesion of bacterial and mammalian cells. *Langmuir* 17: 6336–6343.
4. Pham T, Lai D, Ji D, et al. (2004) Well-ordered self-assembled monolayer surfaces can be used to enhance the growth of protein crystals. *Colloid Surface B* 34: 191–196.
5. Shakiba A, Patil SL, Zenasni O, et al. (2017) DNA loading and release using custom-tailored poly(L-lysine) surfaces. *ACS Appl Mater Interfaces* 9: 23370–23378.
6. Nuzzo RG, Dubois LH, Allara DL (1990) Fundamental studies of microscopic wetting on organic surfaces. 1. formation and structural characterization of a self-consistent series of polyfunctional organic monolayers. *J Am Chem Soc* 112: 558–569.
7. Kim HI, Graupe M, Oloba O, et al. (1999) Molecularly specific studies of the frictional properties of monolayer films: a systematic comparison of CF_3-, $(CH_3)_2CH$-, and CH_3-terminated Films. *Langmuir* 15: 3179–3185.
8. Love JC, Estroff LA, Kriebel JK, et al. (2005) Self-assembled monolayers of thiolates on metals as a form of nanotechnology. *Chem Rev* 105: 1103–1169.
9. Chinwangso P, Lee HJ, Jamison AC, et al. (2017) Structure, wettability, and thermal stability of organic thin-films on gold generated from the molecular self-assembly of unsymmetrical oligo(ethylene glycol) spiroalkanedithiols. *Langmuir* 33: 1751–1762.
10. Marquez MD, Zenasni O, Jamison AC, et al. (2017) Homogeneously mixed monolayers: emergence of compositionally conflicted interfaces. *Langmuir* 33: 8839–8855.
11. Rittikulsittichai S, Park CS, Jamison AC, et al. (2017) Bidentate aromatic thiols on gold: new insight regarding the influence of branching on the structure, packing, wetting, and stability of self-assembled monolayers on gold surfaces. *Langmuir* 33: 4396–4406.

12. Park CS, Lee HJ, Jamison AC, et al. (2016) Robust thick polymer brushes grafted from gold surfaces using bidentate thiol-based atom-transfer radical polymerization initiators. *ACS Appl Mater Interfaces* 8: 5586–5594.
13. Schreiber F (2000) Structure and growth of self-assembling monolayers. *Prog Surf Sci* 65: 151–257.
14. Chen S, Zheng J, Li L, et al. (2005) Strong resistance of phosphorylcholine self-assembled monolayers to protein adsorption: insights into nonfouling properties of zwitterionic materials. *J Am Chem Soc* 127: 14473–14478.
15. Arima Y, Iwata H (2007) Effect of wettability and surface functional groups on protein adsorption and cell adhesion using well-defined mixed self-assembled monolayers. *Biomaterials* 28: 3074–3082.
16. Nanda D, Varshney P, Satapathy M, et al. (2017) Self-assembled monolayer of functionalized silica microparticles for self-cleaning applications. *Colloid Surface A* 529: 231–238.
17. Laibinis PE, Whitesides GM, Allara DL, et al. (1991) Comparison of the structures and wetting properties of self-assembled monolayers of n-alkanethiols on the coinage metal surfaces, copper, silver, and gold. *J Am Chem Soc* 113: 7152–7167.
18. Colorado R, Lee TR (2000) Physical organic probes of interfacial wettability reveal the importance of surface dipole effect. *J Phys Org Chem* 13: 796–807.
19. Baghbanzadeh M, Simeone FC, Bowers CM, et al. (2014) Odd-even effects in charge transport across *n*-alkanethiolate based SAMs. *J Am Chem Soc* 136: 16919–16925.
20. Lee S, Puck A, Graupe M, et al. (2001) Structure, wettability, and frictional properties of phenyl-terminated self-assembled monolayers on gold. *Langmuir* 17: 7364–7370.
21. Graupe M, Koini T, Kim HI, et al. (1999) Self-assembled monolayers of CF_3-terminated alkanethiols on gold. *Colloid Surface A* 154: 239–244.
22. Krishna DD, Ramakrishnan R, Sundararajan U, et al. (2006) A simple technique to grow polymer brushes using in situ surface ligation of an organometallic initiator. *J Am Chem Soc* 128: 13040–13041.
23. Meyerbröker N, Zharnikov M (2012) Modification of nitrile-terminated biphenylthiol self-assembled monolayers by electron irradiation and related applications. *Langmuir* 28: 9583–9592.
24. Bain CD, Troughton EB, Tao YT, et al. (1989) Formation of monolayer films by the spontaneous assembly of organic thiols from solution onto gold. *J Am Chem Soc* 111: 321–335.
25. Fenter P, Eberhardt A, Liang KS, et al. (1997) Epitaxy and chain length dependent strain in self-assembled monolayers. *J Chem Phys* 106: 1600–1608.
26. Frey S, Shaporenko A, Zharnikov M, et al. (2003) Self-assembled monolayers of nitrile-functionalized alkanethiols on gold and silver substrates. *J Phys Chem B* 107: 7716–7725.
27. Hautman J, Bareman JP, Mar W, et al. (1991) Molecular dynamics investigations of self-assembled monolayers. *J Chem Soc Faraday Trans* 87: 2031–2037.
28. Law KY (2013) Definitions for Hydrophilicity, Hydrophobicity, and Superhydrophobicity: Getting the Basics Right. *J Phys Chem Lett* 1: 57–58.
29. Holmlin RE, Chen X, Chapman RG, et al. (2001) Zwitterionic SAMs that resist nonspecific adsorption of protein from aqueous buffer. *Langmuir* 17: 2841–2850.

30. Lee HJ, Jamison AC, Lee TR (2015) Boc-protected ω-amino alkanedithiols provide chemically and thermally stable amine-terminated monolayers on gold. *Langmuir* 31: 2136–2146.
31. Engquist I, Lestelius M, Liedberg B (1997) Microscopic wettability of ester- and acetate-terminated self-assembled monolayers. *Langmuir* 13: 4003–4012.
32. Allara DL, Nuzzo RG (1985) Spontaneously organized molecular assemblies. 1. Formation, dynamics, and physical properties of *n*-alkanoic acids adsorbed from solution on an oxidized aluminum surface. *Langmuir* 1: 45–52.
33. Porter MD, Bright TB, Allara DL, et al. (1987) Spontaneously organized molecular assemblies. 4. Structural characterization of *n*-alkyl thiol monolayers on gold by optical ellipsometry, infrared spectroscopy, and electrochemistry. *J Am Chem Soc* 109: 3559–3568.
34. Snyder RG, Strauss HL, Elliger CA (1982) Carbon-hydrogen stretching modes and the structure of *n*-alkyl chains. 1. Long, disordered chains. *J Phys Chem* 86: 5145–5150.
35. Sellers H, Ulman A, Shnidman Y, et al. (1993) Structure and Binding of Alkanethiolates on Gold and Silver Surfaces: Implications for Self-Assembled Monolayers. *J Am Chem Soc* 115: 9389–9401.
36. Castner DG, Hinds K, Grainger DW (1996) X-ray photoelectron spectroscopy sulfur 2p study of organic thiol and disulfide binding interactions with gold surfaces. *Langmuir* 12: 5083–5086.
37. Ågren H, Carravetta V, Vahtras O, et al. (1994) Direct, atomic orbital, static exchange calculations of photoabsorption spectra of large molecules and clusters. *Chem Phys Lett* 222: 75–81.
38. Widrig CA, Chung C, Porter MD, et al. (1991) The Electrochemical desorption of n-alkanethiol monolayers from polycrystalline Au and Ag electrodes. *J Electroanal Chem Interfacial Electrochem* 310: 335–359.
39. Kondoh H, Kodama C, Sumida H, et al. (1999) Molecular processes of adsorption and desorption of alkanethiol monolayers on Au(111). *J Chem Phys* 111: 1175–1184.
40. Hutt DA, Leggett GJ (1996) Influence of adsorbate ordering on rates of UV photooxidation of self-assembled monolayers. *J Phys Chem* 100: 6657–6662.
41. Bain CD, Whitesides GM (1989) Attenuation lengths of photoelectrons in hydrocarbon films. *J Phys Chem* 93: 1670–1673.
42. Lee S, Shon YS, Colorado R, et al. (2000) The influence of packing densities and surface order on the frictional properties of alkanethiol self-assembled monolayers (SAMs) on gold: a comparison of SAMs derived from normal and spiroalkanedithiols. *Langmuir* 16: 2220–2224.
43. Shon YS, Colorado R, Williams CT, et al. (2000) Low-density self-assembled monolayers on gold derived from chelating 2-monoalkylpropane-1,3-dithiols. *Langmuir* 16: 541–548.
44. Park JS, Smith AC, Lee TR (2004) Loosely packed self-assembled monolayers on gold generated from 2-alkyl-2-methylpropane-1,3-dithiols. *Langmuir* 20: 5829–5836.

AIMS Press